

## Systematic study of Bh isotopes in a relativistic mean field formalism

M. S. Mehta,<sup>1</sup> B. K. Raj,<sup>2</sup> S. K. Patra,<sup>3</sup> and Raj K. Gupta<sup>1</sup>

<sup>1</sup>*Department of Physics, Panjab University, Chandigarh 160 014, India*

<sup>2</sup>*Department of Physics, BJB College, Bhubaneswar 751 014, India*

<sup>3</sup>*Institute of Physics, Sachivalaya Marg, Bhubaneswar 751 005, India*

(Received 25 June 2002; published 29 October 2002)

The binding energy, charge radius, and quadrupole deformation parameter for the isotopic chain of the superheavy element bohrium ( $_{107}\text{Bh}$ ), from proton to neutron drip line, are calculated by using an axially deformed relativistic mean field model. The potential energy surfaces for some of the selected nuclei are plotted and the various possible shapes are investigated. The rms radii, density distributions, and two-neutron separation energies are also evaluated and the single-particle energies for some illustrative cases are analyzed to see the magic structures. Furthermore, the  $\alpha$ -decay rates are calculated and compared with the available experimental data for the recently observed new isotopes  $^{266,267}\text{Bh}$ .

DOI: 10.1103/PhysRevC.66.044317

PACS number(s): 21.10.Dr, 21.10.Tg, 21.60.Fw

### I. INTRODUCTION

The bohrium nucleus ( $Z=107$ , Bh) was first identified as the isotope  $^{262}\text{Bh}$ , produced in  $^{209}\text{Bi}(^{54}\text{Cr},n)$  reaction [1]. Until recently, experimentally the decay properties of only the  $^{261,262,264}\text{Bh}$  isotopes were known. For  $Z<107$  nuclei, the electronic configurations are well studied due to the longer lifetimes ( $>1$  s) of these nuclei [2]. However, the chemistry of elements  $Z=107$  and  $Z=108$  were unknown and the prospects of the chemical studies for these next transactinide elements did not look promising. Nevertheless, gas phase chemistry with the lighter homologs Re and Os has been known for quite some time [3–7] and the search for the long-lived isotopes of element  $Z=107$  was based on these methods [5,6]. Recently, Wilk *et al.* [8] have identified the neutron-rich  $^{266,267}\text{Bh}$  isotopes and estimated their half-life times  $\sim 1$  s and  $17_{-6}^{+14}$  s, respectively. Thus, the relatively longer lifetime of  $^{267}\text{Bh}$  makes possible to study now the electronic structure of the Bh nucleus and test the available theoretical methods for calculating their structure and decay properties. We do this here for the first time for the relativistic mean field (RMF) method by considering a complete isotopic chain of Bh (115 cases) from proton to neutron drip lines. The RMF calculations for some superheavy elements have been made earlier [9,10] but then only a few even-even isotopes were considered. In the present calculation for Bh, we include not only a large number of isotopes of Bh but also both the odd- and even- $A$  isotopes are considered.

Since we are considering here a larger set of Bh nuclei between the proton and neutron drip lines, i.e., both very neutron-deficient and very neutron-rich isotopes of Bh, this study is expected to throw some light on the magicity of neutron numbers beyond  $N=126$  in the superheavy region. In other words, in our analysis of Bh nuclei with  $N=144$ – $258$ , we are likely to pass through some spherical or deformed neutron magic numbers, which in recent years have been predicted to be different for different model calculations [9–12]. More than 30 years ago [13], it was predicted that the next doubly magic nucleus beyond  $Z=82$ ,  $N=126$ ,  $^{208}\text{Pb}$  is  $^{298}_{184}114$  and that nuclei in its vicinity, on an

island of superheavy nuclei, have half-lives of of the order of  $10^9$  years [14]. The same result is supported by some recent calculations [15]. Also, the  $Z=114$  nucleus is now synthesized but for only a lighter isotope  $^{289}_{175}114$  [16] whose  $\alpha$ -decay chain is observed and the  $\alpha$ -decay energies or  $Q_\alpha$  values are explained on a RMF calculation [10]. More recently, the calculations for superheavy elements have generated quite an excitement where new magic numbers are predicted for both protons and neutrons. In a spherical relativistic mean field calculation, using the various parameter sets, Rutz *et al.* [11] studied a wide range of nuclei in the superheavy region and predicted  $Z=120$  and  $N=172$  as the next spherical magic shells. In the other, rather complete, deformed relativistic mean field calculation, we [9,17] predicted  $Z=120$  and  $N=184$  as the next possible magic numbers in the superheavy region for use of various parameter sets. The role of shell effects in the stability of nuclei at  $Z=120$  was first pointed out by one of us and others [17], predicting  $^{94}\text{Sr}+^{208}\text{Pb}$  as the best cold fusion reaction for producing  $^{302}_{182}120$  nucleus. Note that  $^{94}\text{Sr}$  is a deformed nucleus and the use of spherical  $^{88}_{38}\text{Sr}_{50}$  for a lighter isotope of  $Z=120$  will be of further advantage in a cold fusion reaction [18]. Also,  $Z=126$  and  $N=184$  as the proton and neutron magic numbers are predicted for use of both the Skyrme-Hartree-Fock method with a density-independent contact pairing interaction and the macro-microscopic model with monopole pairing interaction [12]. Furthermore, a maximum stabilization against spontaneous fission is expected both empirically and theoretically for the deformed  $_{108}\text{Hs}$  nucleus with  $N=162$  [19,20]. Also, a spherical shell magicity is noted empirically at  $N=152$  [19]. The deformed magicity for  $^{270}_{108}\text{Hs}$  is of more relevance to our study here since the Bh nucleus has only one proton less than the Hs nucleus.

The deformed relativistic mean field (DRMF) calculations are known to give an excellent description of nuclei both in the region of proton and neutron drip lines. Also, it reproduces very well the possible *breaking* of known spherical shell closures [21]. For the superheavy elements, our recent work [9,10] shows that the DRMF model predicts their bind-

ing energies (the only measured quantity so far for the superheavy nuclei) best for the NL3 force parameter set [22]. It may be noted that the RMF parameter sets are determined by fitting nuclear matter properties, neutron-proton asymmetry energies, root-mean-square (rms) radii and the binding energies of some spherical nuclei, and then no further adjustment is to be made in these parameters of the Lagrangian. The predictive power of the relativistic mean field parametrizations is well known and some examples can be found, e.g., in Refs. [9,23] and the references quoted therein.

The paper is organized as follows: In Sec. II we outline the essential formalism for the relativistic mean field method and its Lagrangian. The results of our calculations for Bh isotopes are discussed in Sec. III. The calculations are made for the binding energies, rms radii, quadrupole moments, the two neutron separation energies, and the single-particle energies. The last two quantities allow us to predict the possible neutron and proton magic numbers in the superheavy valley. Also, the potential energy surfaces, density distributions, and  $Q_\alpha$  values are calculated. Finally a summary of our results and conclusions are given in Sec. IV.

## II. THE FORMALISM

The relativistic mean field approach is well known and, its theory being well documented, we skip all the details which can be found in Refs. [24–30]. Here, we start with the relativistic Lagrangian density for a nucleon-meson many-body system,

$$\begin{aligned} \mathcal{L} = & \bar{\psi}_i \{ i \gamma^\mu \partial_\mu - M \} \psi_i + \frac{1}{2} \partial^\mu \sigma \partial_\mu \sigma - \frac{1}{2} m_\sigma^2 \sigma^2 - \frac{1}{3} g_2 \sigma^3 \\ & - \frac{1}{4} g_3 \sigma^4 - g_s \bar{\psi}_i \psi_i \sigma - \frac{1}{4} \Omega^{\mu\nu} \Omega_{\mu\nu} + \frac{1}{2} m_\omega^2 V^\mu V_\mu \\ & + \frac{1}{4} c_3 (V_\mu V^\mu)^2 - g_w \bar{\psi}_i \gamma^\mu \psi_i V_\mu - \frac{1}{4} \vec{B}^{\mu\nu} \cdot \vec{B}_{\mu\nu} \\ & + \frac{1}{2} m_\rho^2 \vec{R}^\mu \cdot \vec{R}_\mu - g_\rho \bar{\psi}_i \gamma^\mu \vec{\tau} \psi_i \cdot \vec{R}_\mu - \frac{1}{4} F^{\mu\nu} F_{\mu\nu} \\ & - e \bar{\psi}_i \gamma^\mu \frac{(1 - \tau_{3i})}{2} \psi_i A_\mu. \end{aligned} \quad (1)$$

The field for the  $\sigma$  meson is denoted by  $\sigma$ , that for the  $\omega$  meson by  $V_\mu$ , and for the isovector  $\rho$  meson by  $\vec{R}_\mu$ .  $A^\mu$  denotes the electromagnetic field. The  $\psi_i$  are the Dirac spinors for the nucleons whose third component of isospin is denoted by  $\tau_{3i}$ . Here  $g_s$ ,  $g_w$ ,  $g_\rho$ , and  $e^2/4\pi = \frac{1}{137}$  are the coupling constants for  $\sigma$ ,  $\omega$ ,  $\rho$ , mesons, and photon, respectively. The  $g_2$ ,  $g_3$ , and  $c_3$  are the parameters for the nonlinear terms of  $\sigma$  and  $\omega$  mesons.  $M$  is the mass of the nucleon and  $m_\sigma$ ,  $m_\omega$ , and  $m_\rho$  are the masses of the  $\sigma$ ,  $\omega$ , and  $\rho$  mesons, respectively.  $\Omega^{\mu\nu}$ ,  $\vec{B}^{\mu\nu}$ , and  $F^{\mu\nu}$  are the field tensors for the  $V^\mu$ ,  $\vec{R}^\mu$ , and the photon fields, respectively [25].

From the relativistic Lagrangian we get the field equations for the nucleons and mesons. These equations are solved by expanding the upper and lower components of the Dirac spinors and the Boson fields in a deformed harmonic oscillator basis with an initial deformation. The set of coupled equations is solved numerically by a self-consistent iteration method. The center-of-mass motion is estimated by the usual

harmonic oscillator formula  $E_{c.m.} = \frac{3}{4}(41A^{-1/3})$ . The quadrupole deformation parameter  $\beta_2$  is evaluated from the resulting quadrupole moment [25]. The total binding energy and the other observables are also obtained by using the standard relations in, e.g., Refs. [9,25]. The Boson and Fermion wave functions are evaluated with  $N_F = N_B = 20$  major harmonic oscillator shells, which is a reasonably large space for the presently considered superheavy region. The prolate and oblate solutions are evaluated starting with an initial deformation  $\beta_2 = 0.2$  and  $\beta_2 = -0.2$ , respectively. The successful NL3 set [22] is used and the parameter values are taken from Ref. [31].

For our application of the above axially deformed relativistic mean field approach to the ground-state properties of Bh isotopes, we have chosen the NL3 force parameters because, to our knowledge, it has the best predictive power amongst all the RMF parametrizations for finite nuclei [10]. The calculated binding energies also allow us to extract the  $Q_\alpha$  values for the  $\alpha$ -decay chains of these nuclei and we present here the results of our calculations for the two known  $\alpha$ -decay chains of  $^{266,267}\text{Bh}$  nuclei. We have also calculated the potential energy surfaces (PES) of Bh nuclei in a constrained calculation [32–35], i.e., instead of minimizing the  $H_0$ , we have minimized  $H' = H_0 - \lambda Q_2$ , with  $\lambda$  as a Lagrange multiplier and  $Q_2$ , the quadrupole moment.  $H_0$  is the Dirac mean field Hamiltonian (the notations are standard and its form can be seen in Refs. [25,33,35]). In other words, instead of evaluating the free solution of a local minimum, we estimate the constrained binding energy  $E_c$ , i.e., the binding energy of a solution at a given quadrupole deformation. The role of decreasing or increasing the neutron number on the PES is also analyzed.

The calculation of odd-even and odd-odd nuclei in an axially deformed basis is a tough task in the RMF model. To take care of the lone odd nucleon, one has to violate the time-reversal symmetry in the mean field and only the time-like components of the  $V_0$ ,  $b_0$ , and  $A_0$  of the  $\omega$ ,  $\rho$ , and photon fields are retained. The space components of these fields (which are odd under time reversal and parity) are neglected. They are important in the determination of properties such as magnetic moments [36], but have very small effect on the bulk properties, such as the binding energies and quadrupole deformations, and can be neglected to a good approximation [37]. However, in our calculations for the odd nuclei we employ the blocking approximation, which restores the time-reversal symmetry. In this approach one pair of conjugate states  $\pm m$  is taken out of the pairing scheme. The odd particle stays in one of these states and its corresponding conjugate state remains empty. In general one has to block in turn the different states around the Fermi level to find the one that gives the lowest energy configuration of the odd nucleus. In odd-odd nuclei, we have blocked both the odd proton and the odd neutron. In the evaluation of the potential energy surfaces, instead of the blocking approach, we have adopted a simple average  $m$  scheme.

For known nuclei, close to or not too far from the stability line, the BCS approach provides a reasonably good description of the pairing properties. However, in going to nuclei in the vicinity of the drip lines or to the superheavy region the

coupling to the continuum becomes important. It has been shown that the self-consistent treatment of the BCS approximation breaks down when coupling between bound states and states in the continuum takes place [38]. For most of the nuclei in our study, odd-even mass differences are not measured and little (almost nothing) is known about the precise effect of the pairing interaction. It is expected that for odd-even and odd-odd nuclei the effects of pairing are considerably decreased [39]. Therefore, in the present investigation we have chosen to use the BCS formalism with a small constant pairing strength, namely,  $\Delta_n = \Delta_p = 0.5$  MeV. This value of gaps contributes very little to the total binding energy of the nucleus. The results remain unchanged unless the pairing gap is increased considerably. This type of prescription has already been adopted in the past [9,10,17,40,41].

### III. RESULTS AND DISCUSSIONS

For properties, such as the radii of light halo nuclei, that sensitively depend on the spatial extensions of nucleon densities, a more proper treatment of the continuum could certainly be crucial, e.g., by means of the relativistic Hartree-plus-Bogoliubov (RHB) approach [42–44]. In the RHB model, the wave functions of the occupied quasiparticle states have the correct asymptotic behavior. Results of RHB and RMF-BCS calculations are compared in Ref. [44] for neutron-rich nuclei in the deformed  $N=28$  region. The two models predict almost identical binding energies and similar quadrupole deformations, although they differ significantly in their calculated rms radii (larger in the RMF-BCS model). Also, for the deformed odd- $Z$  proton emitters in the  $53 \leq Z \leq 69$  region, this study [44], for use of the NL3 parameter set, shows that for the isotopes  $^{107}\text{I}$ ,  $^{108}\text{I}$ , and  $^{109}\text{I}$ , the odd valence proton occupies a  $[422]3/2^+$  Nilsson orbital and the ground-state quadrupole deformations are  $\beta_2 = 0.15$ ,  $0.16$ , and  $0.16$ , respectively. For comparisons, we have also performed these calculations [45] with the presently used DRMF model and found the same  $[422]3/2^+$  orbital for the three I isotopes, with the corresponding quadrupole deformation parameters  $\beta_2 = 0.17$ ,  $0.18$ , and  $0.19$ , respectively, in a rather good agreement with the more sophisticated RHB calculation mentioned above. This result further strengthens our faith in applying the DRMF model to Bh nuclei.

#### A. Binding energies

We have first calculated the binding energies of the prolate and oblate solutions of Bh isotopes from the proton drip line nucleus  $A=251$  to the neutron drip line nucleus  $A=365$ . Note that the maximum binding energy solution is the ground state and all other solutions are the excited intrinsic states. Our calculated total binding energies (BE) for prolate and oblate solutions are compared in Fig. 1, with the micro-macroscopic finite range droplet model (FRDM) results [41]. From Fig. 1, we notice that the binding energies obtained for the prolate solutions match better with the FRDM results in the lighter mass region. For the heavier mass nuclei, the binding energies of the oblate solutions are closer to the FRDM calculations. This means that a shape change from

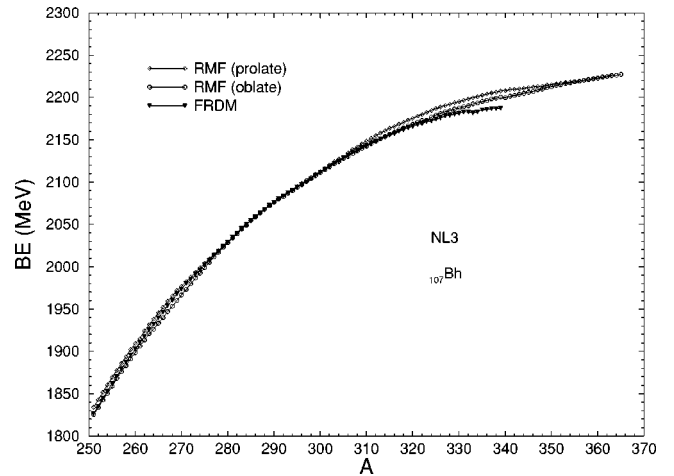


FIG. 1. The calculated total binding energies of the RMF oblate and prolate solutions, compared with the FRDM results.

prolate to oblate occurs while going from lighter to heavier isotopes in the Bh series. This is also evident from Table I where all the calculated data are presented.

In Fig. 2, we have shown the difference between the RMF ground-state solutions and the FRDM binding energies, compared with the difference of RMF oblate and prolate solutions. Apparently, the difference between the two calculations is within  $\sim 1$  MeV for Bh nuclei in the mass range  $A=277$  to  $A=301$ . This difference increases while going toward the lighter as well as heavier mass regions. The maximum difference is rather large,  $\sim 20$  MeV for  $^{339}\text{Bh}$ .

The calculated binding energy per particle ( $BE/A$ ) for both the prolate and oblate solutions is given in Fig. 3, compared with the results of the FRDM [41]. We notice that the DRMF calculations slightly overestimate the  $BE/A$  for some of the isotopes. Also, we find that the isotopes  $^{262}\text{Bh}$  and  $^{263}\text{Bh}$  have the maximum  $BE/A$ . This suggests that these two isotopes are stabler than their neighboring nuclei [9]. However, a recent experiment [8] shows that the half-lives of  $^{266}\text{Bh}$  and  $^{267}\text{Bh}$  are  $\sim 1$  s and  $17_{-6}^{+14}$  s, respectively, whereas the half-life of  $^{262}\text{Bh}$  is only 102 ms. The isotope  $^{263}\text{Bh}$  is yet to be observed [46]. However, the extra stability of  $^{267}\text{Bh}$  could be easily understood on the single-particle shell model picture, discussed below.

#### B. Single-particle energy spectra

It is now well accepted that in the RMF theory [9,10,23,47], the predicted sequence of magic numbers for exotic systems is very much different from that for the normal nuclei. This result seems to be supported by the recent experimental results [48] for light exotic nuclei. Also, the shell closures in the valley of the superheavy island are predicted to be completely different than the traditional ones [9,10,23]. The sequence of magic numbers in the superheavy region is obtained as 80, 92, 120, and 138 for protons (see, e.g., Fig. 4 of Ref. [9]). For  $N > 138$ , the shell gaps appear at  $N=164$ ,  $172$ ,  $184$ ,  $198$ ,  $228$ ,  $258$ , irrespective of the parameter set used. The large gap at  $N \sim 164$  is found to occur for all the superheavy nuclei with  $Z=104$  to  $Z=126$  [10]. The

TABLE I. The ground- and excited-state (e.s.) DRMF results, using NL3 force, for the bulk properties of Bh isotopes. The BE is in MeV and  $r_c$  in femtoseconds.

Nucleus	Case	BE	$\beta_2$	BE/A	$r_c$	Nucleus	Case	BE	$\beta_2$	BE/A	$r_c$
<sup>251</sup> Bh	g.s.	1833.7	0.253	7.306	6.046	<sup>277</sup> Bh	e.s.	2004.9	-0.143	7.264	6.161
	e.s.	1825.3	-0.211	7.272	6.051		g.s.	2014.4	0.175	7.272	6.173
<sup>252</sup> Bh	g.s.	1842.6	0.257	7.312	6.052	<sup>278</sup> Bh	e.s.	2011.3	-0.144	7.261	6.166
	e.s.	1833.5	-0.211	7.276	6.057		g.s.	2019.2	0.167	7.263	6.176
<sup>253</sup> Bh	g.s.	1851.7	0.263	7.319	6.060	<sup>279</sup> Bh	e.s.	2017.0	-0.143	7.255	6.171
	e.s.	1842.3	-0.220	7.282	6.067		g.s.	2024.6	0.153	7.257	6.176
<sup>254</sup> Bh	g.s.	1860.3	0.267	7.324	6.067	<sup>280</sup> Bh	e.s.	2023.1	-0.146	7.251	6.176
	e.s.	1850.2	-0.225	7.284	6.076		g.s.	2029.4	0.143	7.248	6.179
<sup>255</sup> Bh	g.s.	1869.1	0.275	7.330	6.076	<sup>281</sup> Bh	e.s.	2028.2	-0.136	7.243	6.179
	e.s.	1858.5	-0.236	7.288	6.087		g.s.	2034.8	0.129	7.241	6.180
<sup>256</sup> Bh	g.s.	1877.1	0.284	7.332	6.085	<sup>282</sup> Bh	e.s.	2033.8	-0.176	7.238	6.200
	e.s.	1868.1	-0.352	7.297	6.178		g.s.	2039.6	0.113	7.233	6.184
<sup>257</sup> Bh	g.s.	1885.6	0.283	7.337	6.090	<sup>283</sup> Bh	e.s.	2038.5	-0.161	7.229	6.200
	e.s.	1876.1	-0.356	7.300	6.189		g.s.	2044.9	0.107	7.226	6.187
<sup>258</sup> Bh	g.s.	1893.5	0.281	7.339	6.095	<sup>284</sup> Bh	e.s.	2044.2	-0.114	7.223	6.188
	e.s.	1882.9	-0.300	7.298	6.148		g.s.	2049.4	0.099	7.216	6.191
<sup>259</sup> Bh	g.s.	1901.8	0.280	7.343	6.100	<sup>285</sup> Bh	e.s.	2049.0	-0.112	7.215	6.193
	e.s.	1891.0	-0.301	7.301	6.153		g.s.	2054.4	0.086	7.208	6.194
<sup>260</sup> Bh	g.s.	1909.3	0.275	7.343	6.105	<sup>286</sup> Bh	e.s.	2054.4	-0.107	7.208	6.196
	e.s.	1898.4	-0.301	7.302	6.158		g.s.	2058.6	0.074	7.198	6.197
<sup>261</sup> Bh	g.s.	1917.1	0.270	7.345	6.110	<sup>287</sup> Bh	e.s.	2058.8	-0.120	7.198	6.208
	e.s.	1906.2	-0.302	7.303	6.164		g.s.	2063.2	0.065	7.189	6.200
<sup>262</sup> Bh	g.s.	1924.0	0.269	7.344	6.117	<sup>288</sup> Bh	e.s.	2063.6	-0.131	7.190	6.220
	e.s.	1913.1	-0.302	7.302	6.170		g.s.	2067.6	-0.140	7.179	6.233
<sup>263</sup> Bh	g.s.	1931.4	0.267	7.344	6.122	<sup>289</sup> Bh	e.s.	2071.9	-0.135	7.169	6.237
	e.s.	1920.7	-0.309	7.303	6.183		g.s.	2076.2	-0.022	7.159	6.209
<sup>264</sup> Bh	g.s.	1937.9	0.275	7.341	6.131	<sup>290</sup> Bh	e.s.	2080.8	-0.007	7.150	6.212
	e.s.	1926.0	-0.208	7.295	6.110		g.s.	2083.7	-0.024	7.136	6.224
<sup>265</sup> Bh	g.s.	1945.4	0.265	7.341	6.134	<sup>291</sup> Bh	e.s.	2082.5	-0.149	7.132	6.263
	e.s.	1933.2	-0.206	7.295	6.114		g.s.	2087.4	-0.014	7.124	6.230
<sup>266</sup> Bh	g.s.	1951.9	0.272	7.338	6.143	<sup>292</sup> Bh	e.s.	2086.5	-0.182	7.121	6.284
	e.s.	1939.8	-0.199	7.292	6.118		g.s.	2090.7	0.063	7.111	6.243
<sup>267</sup> Bh	g.s.	1959.1	0.273	7.337	6.149	<sup>293</sup> Bh	e.s.	2089.7	-0.191	7.108	6.295
	e.s.	1946.8	-0.196	7.291	6.123		g.s.	2094.8	0.082	7.101	6.256
<sup>268</sup> Bh	g.s.	1965.4	0.270	7.334	6.154	<sup>294</sup> Bh	e.s.	2093.5	-0.201	7.097	6.308
	e.s.	1953.0	-0.190	7.287	6.126		g.s.	2098.3	0.091	7.089	6.267
<sup>269</sup> Bh	g.s.	1971.8	0.266	7.330	6.158	<sup>295</sup> Bh	e.s.	2096.8	-0.209	7.084	6.320
	e.s.	1960.0	-0.184	7.286	6.131		g.s.	2102.2	0.098	7.078	6.277
<sup>270</sup> Bh	g.s.	1976.8	0.262	7.321	6.163	<sup>296</sup> Bh	e.s.	2100.5	-0.218	7.072	6.333
	e.s.	1966.4	-0.179	7.283	6.135		g.s.	2105.5	0.103	7.065	6.288
<sup>271</sup> Bh	g.s.	1982.4	0.258	7.315	6.167	<sup>297</sup> Bh	e.s.	2103.6	-0.225	7.059	6.347
	e.s.	1973.2	-0.160	7.281	6.138		g.s.	2109.0	0.108	7.054	6.297
<sup>272</sup> Bh	g.s.	1987.6	0.226	7.307	6.162	<sup>298</sup> Bh	e.s.	2107.5	-0.283	7.049	6.401
	e.s.	1979.5	-0.157	7.278	6.142		g.s.	2111.9	0.136	7.040	6.305
<sup>273</sup> Bh	g.s.	1993.4	0.200	7.302	6.159	<sup>299</sup> Bh	e.s.	2110.8	-0.289	7.036	6.409
	e.s.	1986.3	-0.145	7.276	6.146		g.s.	2115.7	0.164	7.029	6.317
<sup>274</sup> Bh	g.s.	1998.6	0.194	7.294	6.163	<sup>300</sup> Bh	e.s.	2114.5	-0.286	7.025	6.416
	e.s.	1992.5	-0.143	7.272	6.151		g.s.				
<sup>275</sup> Bh	g.s.	2004.1	0.188	7.288	6.167	<sup>301</sup> Bh					
	e.s.	1999.0	-0.142	7.269	6.156						
<sup>276</sup> Bh	g.s.	2009.0	0.183	7.279	6.170						

TABLE I. (Continued.)

Nucleus	Case	BE	$\beta_2$	BE/A	$r_c$	Nucleus	Case	BE	$\beta_2$	BE/A	$r_c$
<sup>302</sup> Bh	g.s.	2120.0	0.278	7.020	6.383	<sup>328</sup> Bh	g.s.	2191.7	0.269	6.682	6.521
	e.s.	2117.6	-0.287	7.012	6.420		e.s.	2184.2	-0.340	6.659	6.613
<sup>303</sup> Bh	g.s.	2124.0	0.276	7.010	6.388	<sup>329</sup> Bh	g.s.	2193.6	0.266	6.668	6.526
	e.s.	2121.2	-0.291	7.001	6.429		e.s.	2186.0	-0.341	6.644	6.621
<sup>304</sup> Bh	g.s.	2127.3	0.264	6.998	6.388	<sup>330</sup> Bh	g.s.	2195.0	0.272	6.651	6.536
	e.s.	2124.2	-0.295	6.987	6.438		e.s.	2187.2	-0.339	6.628	6.625
<sup>305</sup> Bh	g.s.	2131.1	0.266	6.987	6.394	<sup>331</sup> Bh	g.s.	2196.7	0.269	6.637	6.541
	e.s.	2127.5	-0.298	6.976	6.444		e.s.	2188.9	-0.334	6.613	6.627
<sup>306</sup> Bh	g.s.	2134.5	0.263	6.975	6.398	<sup>332</sup> Bh	g.s.	2197.9	0.266	6.620	6.546
	e.s.	2130.3	-0.302	6.962	6.452		e.s.	2190.1	-0.315	6.597	6.617
<sup>307</sup> Bh	g.s.	2138.2	0.261	6.965	6.402	<sup>333</sup> Bh	g.s.	2199.6	0.263	6.605	6.552
	e.s.	2133.6	-0.306	6.950	6.459		e.s.	2192.0	-0.306	6.583	6.617
<sup>308</sup> Bh	g.s.	2141.5	0.261	6.953	6.408	<sup>334</sup> Bh	g.s.	2200.9	0.260	6.589	6.557
	e.s.	2136.4	-0.310	6.936	6.466		e.s.	2193.3	-0.304	6.567	6.621
<sup>309</sup> Bh	g.s.	2145.1	0.261	6.942	6.414	<sup>335</sup> Bh	g.s.	2202.5	0.257	6.575	6.561
	e.s.	2139.6	-0.314	6.924	6.473		e.s.	2195.1	-0.301	6.553	6.625
<sup>310</sup> Bh	g.s.	2148.0	0.268	6.929	6.424	<sup>336</sup> Bh	g.s.	2203.6	0.254	6.558	6.566
	e.s.	2142.3	-0.316	6.911	6.479		e.s.	2196.3	-0.300	6.537	6.629
<sup>311</sup> Bh	g.s.	2151.7	0.265	6.919	6.427	<sup>337</sup> Bh	g.s.	2205.1	0.251	6.544	6.571
	e.s.	2145.5	-0.321	6.899	6.486		e.s.	2198.0	-0.299	6.522	6.634
<sup>312</sup> Bh	g.s.	2154.6	0.266	6.906	6.433	<sup>338</sup> Bh	g.s.	2206.1	0.248	6.527	6.575
	e.s.	2148.1	-0.323	6.885	6.493		e.s.	2199.0	-0.298	6.506	6.640
<sup>313</sup> Bh	g.s.	2157.9	0.270	6.894	6.441	<sup>339</sup> Bh	g.s.	2207.6	0.245	6.512	6.581
	e.s.	2151.1	-0.324	6.873	6.500		e.s.	2200.5	-0.298	6.491	6.645
<sup>314</sup> Bh	g.s.	2160.5	0.271	6.881	6.447	<sup>340</sup> Bh	g.s.	2207.9	0.240	6.494	6.583
	e.s.	2153.6	-0.326	6.859	6.506		e.s.	2199.7	-0.208	6.470	6.576
<sup>315</sup> Bh	g.s.	2163.5	0.273	6.868	6.453	<sup>341</sup> Bh	g.s.	2209.0	0.238	6.478	6.589
	e.s.	2156.5	-0.327	6.846	6.513		e.s.	2201.2	-0.206	6.455	6.582
<sup>316</sup> Bh	g.s.	2165.6	0.270	6.853	6.459	<sup>342</sup> Bh	g.s.	2209.3	0.234	6.460	6.592
	e.s.	2158.7	-0.329	6.831	6.519		e.s.	2202.2	-0.200	6.439	6.585
<sup>317</sup> Bh	g.s.	2168.3	0.274	6.840	6.465	<sup>343</sup> Bh	g.s.	2210.0	0.230	6.443	6.595
	e.s.	2161.5	-0.330	6.819	6.526		e.s.	2203.6	-0.194	6.425	6.589
<sup>318</sup> Bh	g.s.	2170.4	0.269	6.825	6.464	<sup>344</sup> Bh	g.s.	2210.5	0.196	6.426	6.595
	e.s.	2163.6	-0.331	6.804	6.532		e.s.	2204.6	-0.189	6.409	6.593
<sup>319</sup> Bh	g.s.	2173.0	0.269	6.812	6.471	<sup>345</sup> Bh	g.s.	2211.5	0.190	6.410	6.599
	e.s.	2166.2	-0.331	6.791	6.539		e.s.	2206.1	-0.180	6.394	6.595
<sup>320</sup> Bh	g.s.	2175.1	0.271	6.797	6.478	<sup>346</sup> Bh	g.s.	2211.9	0.182	6.393	6.601
	e.s.	2168.2	-0.332	6.776	6.546		e.s.	2207.1	-0.174	6.379	6.598
<sup>321</sup> Bh	g.s.	2177.7	0.273	6.784	6.485	<sup>347</sup> Bh	g.s.	2212.9	0.177	6.377	6.604
	e.s.	2170.8	-0.333	6.762	6.553		e.s.	2208.7	-0.167	6.365	6.602
<sup>322</sup> Bh	g.s.	2179.7	0.274	6.769	6.491	<sup>348</sup> Bh	g.s.	2213.4	0.172	6.360	6.607
	e.s.	2172.5	-0.334	6.747	6.562		e.s.	2209.8	-0.157	6.350	6.608
<sup>323</sup> Bh	g.s.	2182.4	0.270	6.757	6.492	<sup>349</sup> Bh	g.s.	2214.4	0.164	6.345	6.610
	e.s.	2172.8	-0.333	6.727	6.563		e.s.	2211.4	-0.152	6.336	6.612
<sup>324</sup> Bh	g.s.	2184.3	0.270	6.742	6.497	<sup>350</sup> Bh	g.s.	2214.9	0.158	6.328	6.613
	e.s.	2176.7	-0.337	6.718	6.581		e.s.	2212.5	-0.147	6.321	6.617
<sup>325</sup> Bh	g.s.	2186.7	0.270	6.728	6.503	<sup>351</sup> Bh	g.s.	2216.0	0.144	6.313	6.617
	e.s.	2179.0	-0.340	6.705	6.591		e.s.	2214.1	-0.142	6.308	6.620
<sup>326</sup> Bh	g.s.	2188.4	0.270	6.713	6.509	<sup>352</sup> Bh	g.s.	2216.6	0.136	6.297	6.621
	e.s.	2180.7	-0.341	6.689	6.600		e.s.	2214.9	-0.136	6.292	6.625
<sup>327</sup> Bh	g.s.	2190.5	0.270	6.699	6.515	<sup>353</sup> Bh	g.s.	2217.7	0.131	6.282	6.623
	e.s.	2182.9	-0.342	6.675	6.609		e.s.	2216.4	-0.131	6.279	6.628

TABLE I. (Continued.)

Nucleus	Case	BE	$\beta_2$	BE/A	$r_c$	Nucleus	Case	BE	$\beta_2$	BE/A	$r_c$
$^{354}\text{Bh}$	g.s.	2217.9	0.120	6.265	6.626	$^{360}\text{Bh}$	g.s.	2222.7	-0.041	6.174	6.651
	e.s.	2217.1	-0.122	6.263	6.630		$^{361}\text{Bh}$	g.s.	2223.9	-0.030	6.160
$^{355}\text{Bh}$	g.s.	2218.7	0.113	6.250	6.628	$^{362}\text{Bh}$		g.s.	2224.6	-0.017	6.145
	e.s.	2218.2	-0.113	6.249	6.633		$^{363}\text{Bh}$	g.s.	2225.8	0.006	6.132
$^{356}\text{Bh}$	g.s.	2219.0	0.103	6.233	6.632	$^{364}\text{Bh}$		g.s.	2226.1	0.003	6.116
	e.s.	2219.0	-0.101	6.233	6.637		$^{365}\text{Bh}$	g.s.	2227.2	0.003	6.102
$^{357}\text{Bh}$	g.s.	2220.2	-0.092	6.219	6.640						
$^{358}\text{Bh}$	g.s.	2220.9	-0.081	6.204	6.643						
$^{359}\text{Bh}$	g.s.	2222.0	-0.071	6.189	6.645						

nonrelativistic model calculations also predict that  $N=162$  is the next possible magic shell [49]. As already mentioned in the Introduction, this is empirically found to be the case for  $Z=108$ ,  $N=162$ ,  $^{270}\text{Hs}$  nucleus and hence could be taken as the possible reason for  $Z=107$ ,  $N=160$ ,  $^{267}\text{Bh}$  to have a longer half-life time than the  $^{262}\text{Bh}$  nucleus, owing to its approaching the  $N=162$  or  $164$  closed shell.

For Bh isotopes, the single-particle energy spectra are illustrated in Fig. 4 for some specific nuclei, the  $^{261,271,291,365}\text{Bh}$ . This means considering prolate, oblate and spherical systems (see Table I). We find reasonably large shell gaps at  $N=2, 8, 18, 34, 50, 58, 92, 120, 138, 164, 184, 198$ , and  $258$  and at  $Z=2, 8, 18, 34, 50, 58, 92, 120$ , and  $138$  for  $^{271,291,365}\text{Bh}$ . The same for  $^{261}\text{Bh}$  are rather weaker (smaller shell gaps) as well as different, though the ground-state deformation for  $^{261}\text{Bh}$  is found to be nearly the same ( $\sim 0.27$ ) as for  $^{271}\text{Bh}$ . The known magic numbers at  $N$  (or  $Z$ ) = 20, 28, and 82 are not obtained for any of the nuclei studied here. Note that the shell gaps at  $Z=120$  and  $138$  are very prominent for  $^{271,291,365}\text{Bh}$  nuclei. We also notice a reasonable gap at  $Z=114$ , predicted earlier in some other RMF calculation [50].

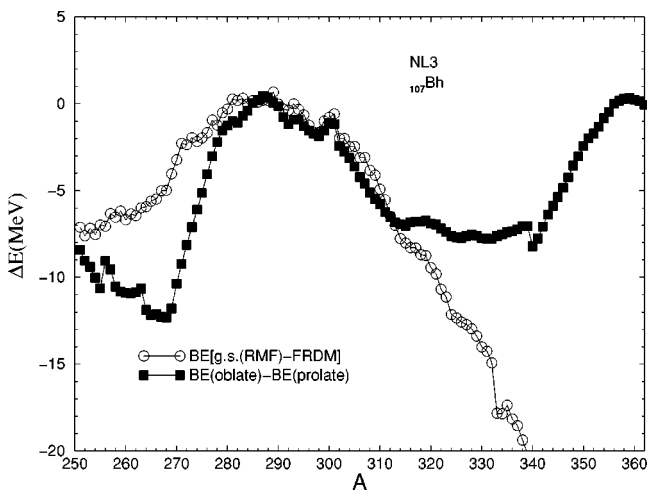


FIG. 2. The difference between the RMF ground-state solution and the FRDM binding energy, compared with that of the RMF prolate and oblate ground-state solutions.

It is relevant to note here that for identifying the magic numbers, it is not sufficient to simply draw the single-particle level scheme and look for gaps. In fact, the level scheme can be quite complicated and the high degree of degeneracy weighs the levels quite unequally. Also, the self-consistency causes a strong coupling of the proton and neutron shell structures. This implies that the proton magic numbers can vary, depending on the number of neutrons present and vice versa. Thus, it is not possible to calculate the energy spectra for one  $(N, Z)$  system as a representative for the whole region of nuclei, rather each nucleus needs a separate evaluation in order to identify the proper combination of magic neutrons for a particular number of protons and vice versa [51]. Hence, in the absence of the Strutinsky type of shell corrections, the  $S_{2n}$  values give a better insight into the shell closure effects of the deformed nuclei [23,39], rather than their deformed single-particle level schemes.

### C. Two-neutron separation energies $S_{2n}$

In order to get a further insight into shell closure effects, we have plotted in Figs. 5 the two-neutron separation energy  $S_{2n}$  for all the Bh isotopes studied here. Figure 5(a) is for

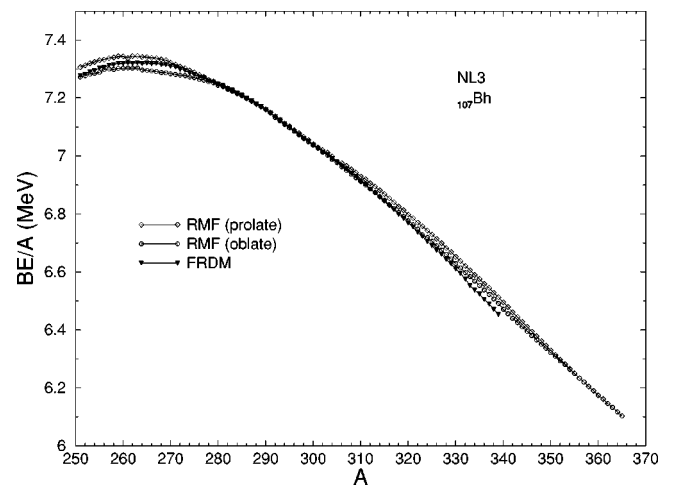


FIG. 3. The binding energy per particle obtained for the prolate and oblate solutions, compared with the FRDM data.

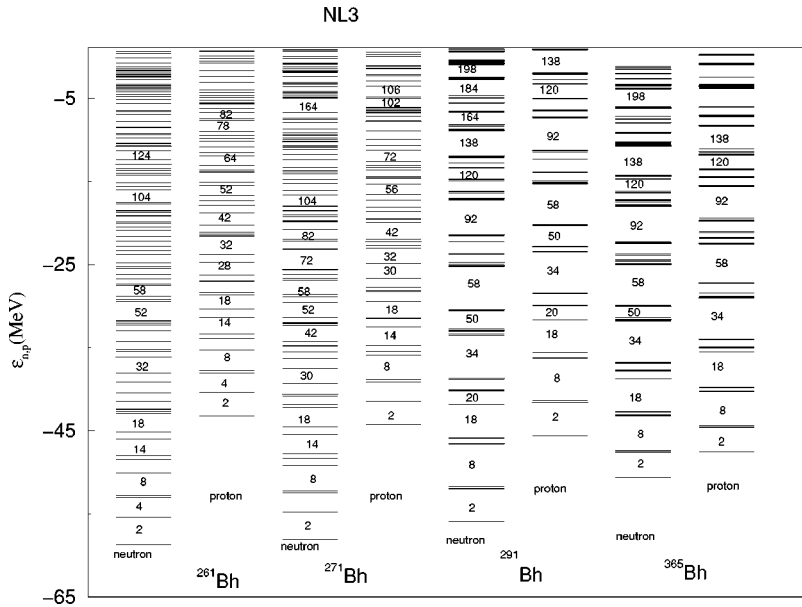


FIG. 4. The RMF ground-state single-particle energy spectra for both protons and neutrons in  $^{261,271,291,365}\text{Bh}$  nuclei.

even- $A$  and Fig. 5(b) for odd- $A$  isotopes. The two-neutron separation energy  $S_{2n}$  is evaluated from the binding energies of the two neighboring isotopes with  $N$  and  $N-2$  neutrons:  $S_{2n}(N,Z) = BE(N,Z) - BE(N-2,Z)$ . Interestingly, the variation of  $S_{2n}$  with  $N$  (or  $A$ ) shows a sudden decrease of  $S_{2n}$  at  $N=152, 162$  (or  $164$ ),  $184, 232$ , and  $258$  for odd- $A$  series and  $N=151, 161$  (or  $163$ ),  $183, 231$ , and  $257$  for even- $A$  series. This clearly favors the magicity of nuclei at the neutron numbers  $N=152, 162$  (or  $164$ ), and  $184$ , in agreement with the predictions of the nonrelativistic model calculations [20,49,52] and experimental systematics [19]. Note that these predictions agree reasonably with the spherical relativistic mean field predictions noted above [10]. Since we are dealing here with deformed nuclei, in a self-consistent calculation, the shell gaps may change by one or two units due to the rearrangement effect. This is in addition to other effects of the self-consistency etc., mentioned earlier.

**D. Potential energy surfaces**

We know from the calculated microscopic energies [20] that the superheavy nuclei are unstable with respect to spontaneous fission. This means that the magnitude of shell energy governs their half-life times. Also, the microscopic energies do not favor spherical shapes for nuclei in the  $Z=107$  region, contrary to the situation for the lighter and heavy  $Z$  elements [10]. In fact, the deformed shell effects play very important role in the description of the superheavy elements. Practically, any deformed gap around the Fermi surface can give rise a local minimum in the PES.

The PES for  $^{262,263,266,267,270}\text{Bh}$  and  $^{280}\text{Bh}$  isotopes are shown in Fig. 6. We find a clear single deep minimum in each nucleus. Also, all the isotopes in the Bh series considered here in Fig. 6 are prolate shaped in the ground state. This can also be seen from Table I where all the calculated bulk properties of Bh nuclei are given. The excited (oblate) shape in each of these Bh nuclei is not clearly defined since the other minimum in the potential energy surface is rather shallow. The oblate minima are found at relatively

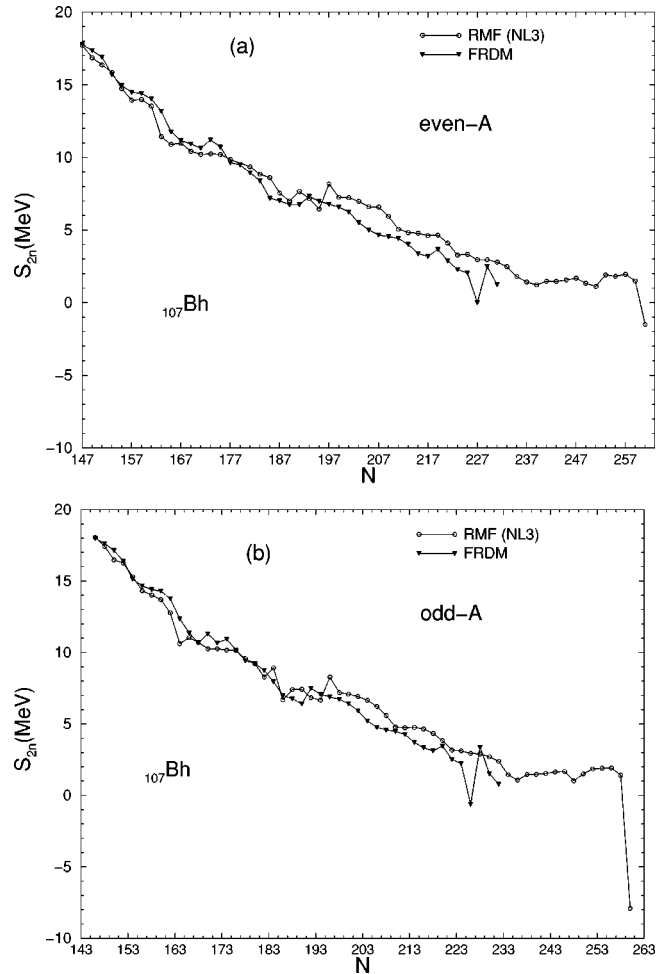


FIG. 5. The RMF results of two-neutron separation energies  $S_{2n}$ , compared with the results of FRDM calculations, (a) is for even- $A$  and (b) for odd- $A$  nuclei.

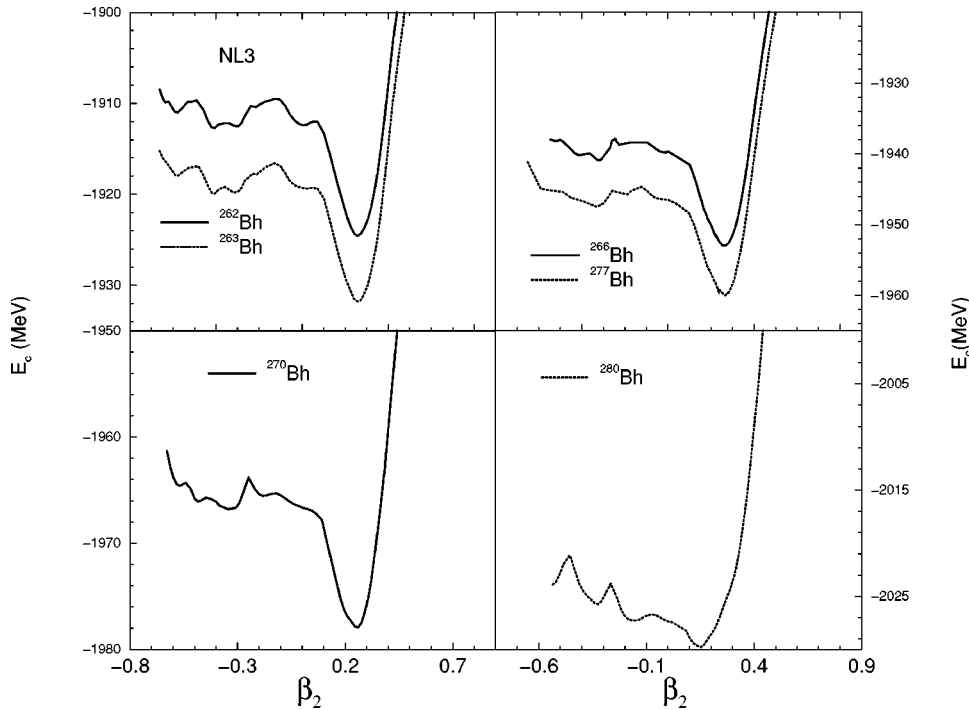


FIG. 6. Potential energy obtained by RMF calculations as a function of the quadrupole deformation parameter  $\beta_2$  for some Bh nuclei.

higher quadrupole deformations ( $\beta_2 \sim -0.3$ ) and are  $\sim 10$ – $12$  MeV higher than the ground-state prolate minima for most of the Bh isotopes, a situation most unlikely for the formation of an excited state (e.s.). However, this type of an excited state is possible when a superheavy nucleus directly undergoes  $\alpha$  decay, without first going to the ground-state configuration. The same pattern is observed in almost all the PES, except for  $^{280}\text{Bh}$  where the oblate minimum is only 1.2 MeV above the ground state, a case almost of shape co-existence observed in many nuclei [23,53]. In some Bh nuclei, the excited-state solution is not at all observed (see Table I for cases of missing e.s. solution).

### E. Quadrupole deformations

The calculated ground-state quadrupole deformation parameter  $\beta_2$  for all Bh isotopes studied here is plotted in Fig. 7 (solid lines with open circles). We notice that the ground-state shape of Bh isotopes changes from prolate to oblate and again from oblate to prolate. Thus, there is a sign change in  $\beta_2$  from positive to negative at  $A=285$  ( $N=178$ ) and again from negative to positive at  $A=294$  ( $N=187$ ). For further increase in mass number of Bh isotopes, we again find a change in sign of the ground-state deformation at mass number  $A=356$  ( $N=249$ ). Also, it can be seen that the magnitude of the ground-state deformation decreases with mass number and there are a bunch of weakly deformed Bh isotopes at  $A \sim 280$ – $300$  and  $A \sim 351$ – $365$ . In other words, we get the nearly spherical Bh nuclei for  $N=173$ – $193$  and  $N=244$ – $258$ . Note that the midshell of these regions of sphericity lie at  $N=184$  and  $252$ . We have also plotted in Fig. 7 the  $\beta_2$  values obtained from the FRDM calculations [41]. We find in general, reasonable agreement between the two results.

### F. Root-mean-square radii

At present it does not seem feasible to measure experimentally the rms charge radii  $r_c$  for the studied Bh nuclei. However, the relatively longer half-life time for  $^{267}\text{Bh}$  raises the hope for the determination of the size of this nucleus in the near future. Also, the estimation of neutron, proton, and matter distribution radii are quite useful from the structure point of view. Therefore, in Fig. 8 we have presented the ground-state neutron  $r_n$ , proton  $r_p$ , charge  $r_{ch}$ , and matter  $r_m$  distribution radii. The interesting result is that the variation of ground-state charge radius with neutron number shows a transition from increase to decrease and then increase at  $N=164$ . The decrease in rms radii occurs in

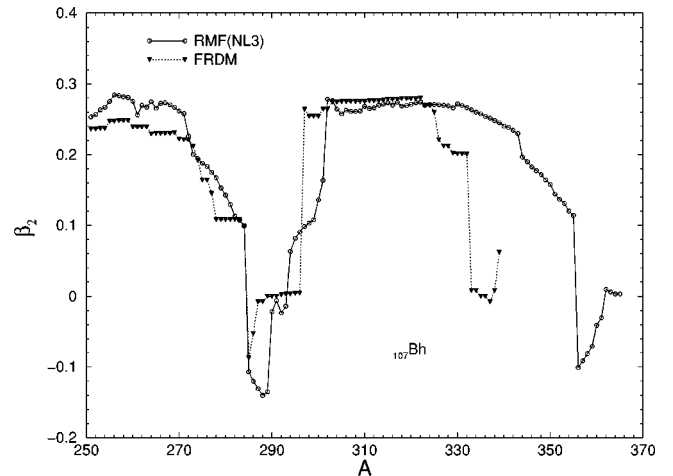


Fig. 7

FIG. 7. The RMF ground-state quadrupole deformation parameter as a function of the mass number of Bh nuclei, compared with the FRDM results.

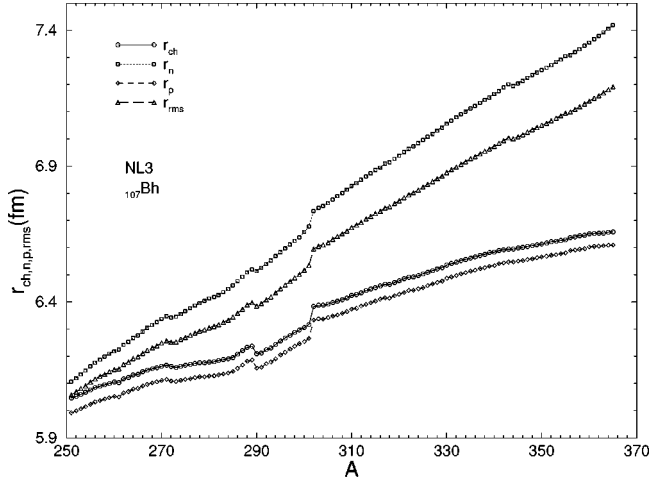


Fig. 8

FIG. 8. The ground neutron  $r_n$ , proton  $r_p$ , charge  $r_c$ , and total mass  $r_m$  radii for Bh series. The charge radii are evaluated taking into account the finite size of the proton, using the relation,  $r_c = \sqrt{r_p^2 + 0.64}$  fm.

the regions of  $N = 164-182$ ,  $183-194$ , and  $N = 237-258$ . This could be taken to mean that the shrinkage in rms radii makes these nuclei spherical and gives the appearance of islands of superheavy nuclei. A similar result is observed in light nuclei [54].

**G. Densities distributions**

The density distributions of protons and neutrons are shown in Fig. 9 for  $^{261,271,291,365}\text{Bh}$  nuclei as the representative cases of the Bh series. For such density distributions, it is clear that the shape of the nuclear potential is more like a modified square well potential. There is a sudden fall in den-

sity beyond  $\sim 5.5$  fm in each case (with rather small skin thicknesses), which could be a possible explanation for the change in magic number sequence. We know that 58, 80, and 92 are the magic numbers for a square well potential, as are also observed in single-particle energy spectra in Fig. 4.

**H.  $Q_\alpha$  values**

Finally, the  $Q_\alpha$  values for  $\alpha$  decays of each of the recently observed  $^{266}\text{Bh}$  and  $^{267}\text{Bh}$  nuclei are calculated by using the relation  $BE(Z, N) = BE(Z-2, N-2) + BE(2, 2) + Q_\alpha$ . Here  $BE(Z, N)$  is the binding energy of the parent nucleus,  $BE(Z-2, N-2)$  of the daughter nucleus, and  $BE(2, 2)$  (28.4 MeV), the experimental binding energy of the  $\alpha$  particle. The calculated results are presented in Table II, along with the recent experimental data [8] and the results of the macro-microscopic FRDM [41] for comparisons. We find that our RMF results are in very good agreement with both the data and the FRDM calculations.

**IV. SUMMARY AND CONCLUSIONS**

In summary, we have calculated the binding energies, the single-particle energy spectra, the rms radii, the neutron and proton density distributions and the quadrupole deformation parameters for Bh isotopes from proton to neutron drip lines, using the axially deformed relativistic mean field approach. The potential energy surfaces are also plotted as a function of the deformation parameter  $\beta_2$ .

The shape of the ground-state configuration changes from prolate to oblate and again from oblate to prolate with the increase of mass number of Bh nucleus. The excited state in most of the cases is found to lie very high. The maximum difference between prolate and oblate solutions is  $\sim 12$  MeV for  $A = 268$ . Also, a spherical (or near spherical) island of Bh nuclei is noticed around  $N = 184$  and 252.

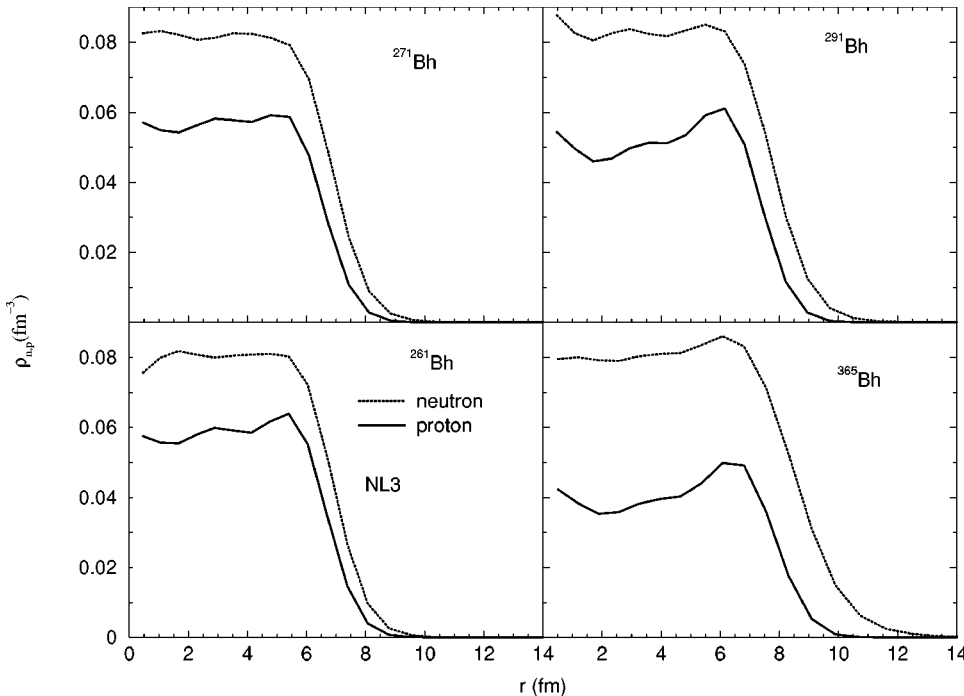


FIG. 9. The density distributions of protons and neutrons in  $^{261,271,291,365}\text{Bh}$  nuclei.

TABLE II. The RMF(NL3) calculated  $Q_\alpha$  energy for each of  $^{266}\text{Bh}$  and  $^{267}\text{Bh}$  nuclei, compared with the experimental data [8] and the FRDM calculation [41]. All energies are in MeV.

Nucleus	$Q_\alpha$ (RMF)	$Q_\alpha$ (Expt.)	$Q_\alpha$ (FRDM)	Nucleus	$Q_\alpha$ (RMF)	$Q_\alpha$ (Expt.)	$Q_\alpha$ (FRDM)
$^{266}\text{Bh}$	9.175	9.29	8.82	$^{267}\text{Bh}$	8.843	8.83	7.52
$^{262}\text{Db}$	8.233	8.45	8.81	$^{263}\text{Db}$	7.823	8.35	8.28
$^{258}\text{Lr}$	7.702	8.60	7.34	$^{259}\text{Lr}$	7.400	8.45	6.94

The magic number sequence is found changed from the standard one, and this sequence in our calculations is  $N = 2, 8, 18, 34, 50, 58, 92, 120, 138, 164, 184, 198, \text{ and } 258$  and  $Z = 2, 8, 18, 34, 50, 58, 92, 120, \text{ and } 138$ . This means that the known magic numbers at  $Z = 20, 28, \text{ and } 82$  are not obtained and some new magic numbers appear. The shell gaps at  $Z = 120$  and  $Z = 138$  are rather prominent for the  $^{271,291,365}\text{Bh}$  nuclei. We also notice a reasonable shell gap at  $Z = 114$ . The obtained magic number sequence is more like that for the square-well potential which is mostly due to the square-well-like shape of the calculated density distributions. The calculated two-neutron separation energies also confirm the above shell gaps obtained in the single-particle energy spectra. The interesting result is that almost all the calculated quantities point to a shell gap at about  $N = 162$  or  $164$ , which means that, in agreement with the empirical trends,  $^{269}\text{Bh}$  or  $^{271}\text{Bh}$  is a most stable nucleus in the chain of Bh-nuclei studied here.

The calculated  $Q_\alpha$  energies, compared with the recently observed data for  $^{266}\text{Bh}$  and  $^{267}\text{Bh}$  isotopes and the FRDM calculations, are found to be somewhat closer to experiments than to the FRDM results.

Finally, it may be noted here that in the present calculations, made in the relativistic mean field approximation, several important factors have been neglected, e.g., we have taken a very rough value of the pairing gaps for both the protons and neutrons in the BCS calculations used for taking the pairing correlations into account. It is also known that the simple BCS approximation breaks down near the drip lines. At present it is quite unknown about the definite pairing gaps

for protons and neutrons in the superheavy region. This calls for the use of an improved treatment of the pairing, beyond a simple BCS, for this region of nuclei. Another approximation is the zero contribution of pions in the present calculations. In the original Walecka model, at the level of RMF approximation, the contribution of pions is taken as zero due to the assumption of spherical shapes of nuclei and also assuming the spin-isospin saturation. The contribution of pions, however, is nonzero in the higher-order approximations (i.e., beyond RMF, as for the inclusion of exchange contribution) [24,55]. Although the pion contribution is non-negligible for the present cases due to the highly asymmetric isotopes, here we have neglected this contribution. Of course, one can readjust the parameters of the Lagrangian to reproduce the experimental observables. In any case, in order to get a quantitative result the above points need to be included in future in these calculations, as is advocated by Toki *et al.* [56]. Work in this direction is in progress and will be published somewhere else.

#### ACKNOWLEDGMENTS

One of the authors (R.K.G.) is grateful to the Council of Scientific and Industrial Research (CSIR), New Delhi. M.S.M. thanks the Institute of Physics, Bhubaneswar, for kind hospitality. B.K.R. thanks the Department of Higher Education, Government of Orissa, the University Grants Commission (UGC), New Delhi, and the Institute of Physics, Bhubaneswar, respectively, for the grant of leave, financial support, and allowing the use of the computer and library facilities.

- 
- [1] G. M $\ddot{u}$ nzenberg, S. Hofmann, F.P. Hessberger, W. Reisdorf, K.-H. Schmidt, J.H.R. Schneider, and P. Armbruster, *Z. Phys. A* **300**, 107 (1981).
- [2] J.V. Kratz, in *Heavy Elements and Related New Phenomena*, edited W. Greiner and R.K. Gupta (World Scientific, Singapore, 1999), Vol. I, Chap. 4, p.129.
- [3] B. Bayar, I. Votsilka, N.G. Zaitseva, and A.F. Novgorodov, *Sov. Radiochem.* **16**, 339 (1974).
- [4] V.P. Domanov, S. H $\ddot{u}$ bener, M.R. Shalaevskii, S.N. Timokhin, D.V. Petrov, and I. Zvara, *Sov. Radiochem.* **25**, 23 (1983).
- [5] I. Zvar, V.P. Domanov, S. H $\ddot{u}$ bener, M.R. Shalaevskii, S.N. Timokhin, B.L. Zhuikov, B. Eichler, and G.V. Buklanov, *Sov. Radiochem.* **26**, 72 (1984).
- [6] M. Sch $\ddot{a}$ del, E. J $\ddot{a}$ ger, E. Schimpf, and W. Br $\ddot{u}$ chle, *Radiochim. Acta* **68**, 1 (1995).
- [7] M. Sch $\ddot{a}$ del, E. J $\ddot{a}$ ger, W. Br $\ddot{u}$ chle, K. S $\ddot{u}$ mmerer, E.K. Hulet, J.F. Wild, R.W. Loughheed, R.J. Dougan, and K.J. Moody, *Radiochim. Acta* **68**, 7 (1995).
- [8] P.A. Wilk, K.E. Gregorich, A. T $\ddot{u}$ rler, C.A. Laue, R. Eichler, V. Ninov, J.L. Adams, U.W. Kirbach, M.R. Lane, D.M. Lee, J.B. Patin, D.A. Shaughnessy, D.A. Strellis, H. Nitsche, and D.C. Hoffman, *Phys. Rev. Lett.* **85**, 2697 (2000).
- [9] S.K. Patra, C.-L. Wu, R.K. Gupta, and C.R. Praharaj, *Nucl. Phys. A* **651**, 117 (1999); S.K. Patra and C.R. Praharaj, *Phys. Rev. C* **44**, 2552 (1991).
- [10] S.K. Patra, W. Greiner, and R.K. Gupta, *J. Phys. G* **26**, L65 (2000); **26**, 1569 (2000).
- [11] K. Rutz, M. Bender, T. B $\ddot{u}$ rvenich, T. Schilling, P.-G. Reinhard, J.A. Maruhn, and W. Greiner, *Phys. Rev. C* **56**, 238 (1997).
- [12] S. C $\acute{w}$ io $\acute{k}$ , W. Nazarewicz, and P.-H. Heenen, *Phys. Rev. Lett.* **83**, 1108 (1999); S. C $\acute{w}$ io $\acute{k}$ , J. Dobaczewski, P.-H. Heenen, P. Magierski, and W. Nazarewicz, *Nucl. Phys. A* **611**, 211 (1996).

- [13] W.D. Myers and W.J. Swiatecki, Nucl. Phys. **A81**, 1 (1966); A. Sobiczewski, F.A. Gareev, and B.N. Kalinkin, Phys. Lett. **22**, 500 (1966); S.G. Nilsson *et al.*, Nucl. Phys. **A115**, 545 (1968); U. Mosel and W. Greiner, Z. Phys. **222**, 261 (1969).
- [14] H.W. Meldner, Ark. Fys. **36**, 593 (1967); W.D. Myers and W.J. Swiatecki, *ibid.* **36**, 343 (1967); S.G. Nilsson, J.R. Nix, A. Sobiczewski, Z. Szymanski, S. Wycech, C. Gustafson, I.-L. Lamm, P. Möller, and B. Nilsson, Nucl. Phys. **A131**, 1 (1969); J. R. Nix, Annu. Rev. Nucl. Sci. **22**, 65 (1972); M. Brack, J. Damgaard, A.S. Jensen, H.C. Pauli, V.M. Strutinsky, and C.Y. Wong, Rev. Mod. Phys. **44**, 185 (1972).
- [15] P. Möller and J.R. Nix, J. Phys. G **25**, 119 (1994).
- [16] Yu. Ts. Oganessian *et al.*, Nature (London) **400**, 242 (1999); Phys. Rev. Lett. **83**, 3154 (1999).
- [17] R.K. Gupta, G. Münzenberg, and W. Greiner, J. Phys. G **23**, L13 (1997).
- [18] R.K. Gupta, M. Balasubramaniam, G. Münzenberg, W. Greiner, and W. Scheid, J. Phys. G **27**, 867 (2001).
- [19] Yu. Ts. Oganessian, in *Heavy Elements and Related New Phenomena* (Ref. [2]), Vol. I, Chap. 2, p. 43.
- [20] S. Cwiok and P. Magierski, in *Heavy Elements and Related New Phenomena* (Ref. [2]), Vol. I, Chap. 7, p. 277.
- [21] R.K. Gupta, S.K. Patra, and W. Greiner, Mod. Phys. Lett. A **12**, 1317 (1997).
- [22] G.A. Lalazissis, J. König, and P. Ring, Phys. Rev. C **55**, 540 (1997).
- [23] S.K. Patra, R.K. Gupta, and W. Greiner, Int. J. Mod. Phys. E **6**, 641 (1997).
- [24] C.J. Horowitz and B.D. Serot, Nucl. Phys. **A368**, 503 (1981); B.D. Serot and J.D. Walecka, Adv. Nucl. Phys. **16**, 1 (1986).
- [25] Y.K. Gambhir, P. Ring, and A. Thimet, Ann. Phys. (N.Y.) **198**, 132 (1990).
- [26] C.E. Price and G.E. Walker, Phys. Rev. C **36**, 354 (1987); J. Boguta and A.R. Bodmer, Nucl. Phys. **A292**, 413 (1977).
- [27] P.-G. Reinhard, M. Rufa, J. Maruhn, W. Greiner, and J. Friedrich, Z. Phys. A **323**, 13 (1986).
- [28] P.K. Panda, S.K. Patra, J. Reinhardt, J.A. Maruhn, H. Stöcker, and W. Greiner, Int. J. Mod. Phys. E **6**, 307 (1997).
- [29] S. Gmuca, Nucl. Phys. **A547**, 447 (1992).
- [30] Y. Sugahara and H. Toki, Nucl. Phys. **A579**, 557 (1994).
- [31] M.M. Sharma, A.R. Farhan, and S. Mythili, Phys. Rev. C **61**, 054306 (2000).
- [32] H. Flocard, P. Quentin, and D. Vautherin, Phys. Lett. **46B**, 304 (1973).
- [33] W. Koepf and P. Ring, Phys. Lett. B **212**, 397 (1988).
- [34] P.-G. Reinhard *et al.*, Phys. Lett. B **218**, 277 (1989).
- [35] D. Hirata, H. Toki, I. Tanihata, and P. Ring, Phys. Lett. B **314**, 168 (1993).
- [36] U. Hofmann and P. Ring, Phys. Lett. B **214**, 307 (1988); L.S. Warrier and Y.K. Gambhir, Phys. Rev. C **49**, 871 (1991).
- [37] G.A. Lalazissis, D. Vretenar, and P. Ring, Nucl. Phys. **A650**, 133 (1999).
- [38] J. Dobaczewski, H. Flocard, and J. Treiner, Nucl. Phys. **A422**, 103 (1984); J. Dobaczewski, W. Nazarewicz, T.R. Werner, J.F. Berger, C.R. Chinn, and J. Dechargé, Phys. Rev. C **53**, 2809 (1996).
- [39] A. Bohr and B.R. Mottelson, *Nuclear Structure* (Benjamin, New York, 1969), Vol. I, Chap. 2.
- [40] T.R. Werner, J.A. Sheikh, W. Nazarewicz, M.R. Strayer, A.S. Umar, and M. Misu, Phys. Lett. B **335**, 259 (1994); T.R. Werner, J.A. Sheikh, M. Misu, W. Nazarewicz, J. Rikowska, K. Heeger, A.S. Umar, and M.R. Strayer, Nucl. Phys. **A597**, 327 (1996); S.K. Patra, C.-Li Wu, and C.R. Praharaaj, Mod. Phys. Lett. A **13**, 2743 (1998).
- [41] P. Möller, J.R. Nix, and K.-L. Kratz, At. Data Nucl. Data Tables **66**, 131 (1997); P. Mollar, J.R. Nix, W.D. Myers, and W.J. Swiatecki, *ibid.* **59**, 185 (1995).
- [42] J. Meng and P. Ring, Phys. Rev. Lett. **77**, 3963 (1996); W. Pöschl, D. Vretenar, G.A. Lalazissis, and P. Ring, *ibid.* **79**, 3841 (1997).
- [43] J. Meng, Nucl. Phys. **A635**, 3 (1998).
- [44] G.A. Lalazissis, D. Vretenar, P. Ring, M. Stoitsov, and L.M. Robledo, Phys. Rev. C **60**, 014310 (1999).
- [45] S.K. Patra, M. Del Estal, M. Cintelles, and X. Viñas, Phys. Rev. C **63**, 044321 (2001).
- [46] G. Münzenberg and S. Hofmann, in *Heavy Elements and Related New Phenomena* (Ref. [2]), Chap. 1, p. 9.
- [47] W.-T. Chou, R.F. Casten, and N.V. Zamfir, Phys. Rev. C **51**, 2444 (1995).
- [48] T. Kautzsch, W.B. Walters, M. Hannawald, K.-L. Kratz, V.I. Mishin, V.N. Moeller, I. Kloeckl, V. Sebastian, U. Koester, M. Koizumi, J. Lettry, and H.L. Ravn, Eur. Phys. J. A **9**, 201 (2000).
- [49] Z. Patyk and A. Sobiczewski, Nucl. Phys. **A533**, 132 (1991).
- [50] M. Rashdan, Phys. Rev. C **63**, 044303 (2001).
- [51] P.-G. Reinhard and J.A. Maruhn, in *Heavy Elements and Related New Phenomena* (Ref. [2]), Chap. 8, p. 332.
- [52] A. Sobiczewski, in *Heavy Elements and Related New Phenomena* (Ref. [2]), Chap. 9, p. 374.
- [53] S.K. Patra, B.K. Raj, M.S. Mehta, and R.K. Gupta, Phys. Rev. C **65**, 054323 (2002).
- [54] I. Tanihata, D. Hirata, T. Kobayashi, S. Shimoura, K. Sugimoto, and H. Toki, Phys. Lett. B **289**, 261 (1992).
- [55] R. Brockmann and W. Weise, Phys. Rev. C **16**, 1281 (1977); R. Brockmann, *ibid.* **18**, 1510 (1978).
- [56] H. Toki, S. Sugimoto, and K. Ikeda, nucl-th/0110017.